Journal of Solid State Chemistry 184 (2011) 36–43

Contents lists available at ScienceDirect

Journal of Solid State Chemistry

journal homepage: www.elsevier.com/locate/jssc

Vacancy ordering and oxygen dynamics in oxide ion conducting $La_{1-x}Sr_xGa_{1-x}Mg_xO_{3-x}$ ceramics: ^{71}Ga, ^{25}Mg and ^{17}O NMR

A. Buzlukov [a], A. Trokiner [b], V. Kozhevnikov [c], S. Verkhovskii [a,b,*], A. Yakubovsky [b,d], I. Leonidov [c], A. Gerashenko [a], A. Stepanov [a], I. Baklanova [c], A. Tankeyev [a]

[a] Institute of Metal Physics, Ural Branch of Russian Academy of Sciences, 620041 Ekaterinburg, Russia
[b] LPEM, ESPCI ParisTech, UMR 8213, CNRS, 75005 Paris, France
[c] Institute of Solid State Chemistry, Ural Branch of Russian Academy of Sciences, 620018 Ekaterinburg, Russia
[d] Russian Research Centre "Kurchatov Institute", 123182 Moscow, Russia

ARTICLE INFO

Article history:
Received 5 June 2010
Received in revised form
19 October 2010
Accepted 21 October 2010
Available online 28 October 2010

Keywords:
Sr- and Mg-doped $LaGaO_3$
Ceramics
Perovskite structure
Anion vacancies
NMR ^{71}Ga
^{17}O
^{25}Mg

ABSTRACT

The oxygen vacancies distribution in the rigid lattice and the thermally activated motion of oxygen atoms are studied in $La_{1-x}Sr_xGa_{1-x}Mg_xO_{3-x}$ ($x=0.00$; 0.05; 0.10; 0.15 and 0.20) compounds. For that ^{71}Ga, ^{25}Mg and ^{17}O NMR was performed from 100 K up to 670 K, and ion conductivity measurements were carried out up to 1273 K. The comparison of the electric field gradients at the Ga- and Mg-sites evidences that oxygen vacancies appear exclusively near gallium cations as a species trapped below room temperature in local clusters, $GaO_{5/2}$-□-$GaO_{5/2}$. These clusters decay at higher temperature into mobile constituents of the structural octahedra $Ga(O_{5/6}□_{1/6})_{6/2}$. At the same time, the nearest octahedral oxygen environment of magnesium cations persists at different doping levels. The case of two adjacent vacant anion sites is found highly unlikely within the studied doping range. The thermally activated oxygen motion starts to develop above room temperature as is observed from both the motional narrowing of ^{17}O NMR spectra and the ^{17}O nuclear spin-lattice relaxation rate. The obtained results show that two types of motion exist, a slow motion and a fast one. The former is a long-range diffusion whereas the latter is a local back and forth oxygen jumps between two adjacent anion sites. These sites are strongly differentiated by the probability of the vacancy formation, like the vacant apical site and the occupied equatorial site in the orthorhombic compositions $x < 0.15$.

1. Introduction

In recent years considerable progress was achieved in the synthesis of high quality ceramics based on Sr and Mg co-doped perovskite-like lanthanum gallate $LaGaO_3$. These materials ($La_{1-x}Sr_xGa_{1-y}Mg_yO_{3-(x+y)/2}$ or LSGM hereinafter) exhibit excellent oxygen ion conductivity and are considered as promising electrolytes for solid oxide fuel cells (SOFCs) operating near 800 °C [1–4]. A number of X-ray diffraction studies are known [4–6] that shed light on structural features and their possible relation to fast ion transport in LSGM. It was shown that the average tilt of $GaO_{6/2}$ octahedra tends to decrease with the increase in doping thus providing easier oxygen ion jumps via the "bottle necks" formed by La–Ga–La triangles. Unfortunately, specific cation environment favoring vacant anion sites remains unclear. It is puzzling that, in the orthorhombic phase ($x, y < 0.15$) the oxygen vacancies exhibit a preference to the equatorial O2 sites at $x, y=0.05$ while at heavier doping they tend to reside in the O1 apical sites in $GaO_{6/2}$ octahedrons [6]. Peculiar ordering of oxygen vacancies and formation of local structural clusters with a symmetry lower than that of the surrounding crystal was observed in the pseudo-cubic LSGM ($x=0.20$, $y=0.15$) by neutron and electron diffraction at room temperature [7,8]. Heating results in a decrease and eventual disappearance of the local defect clusters and thus favors the ion conductivity increase [8]. However, these local structural changes are difficult to observe by diffraction techniques. The features of the local structure [9–13] on atomic level and even the character of the movement of oxygen ions [14,15] can be studied in more details by making use of solid state NMR spectroscopy.

In this work we have applied NMR in order to gain insight into oxygen environment of gallium and magnesium and thermally activated movement of oxygen ions up to 670 K in LSGM. The first order quadrupole splitting of ^{71}Ga, ^{25}Mg spectra was studied for elucidation of how respective electric field gradients vary with changes in doping and vacancy concentration. The onset of thermally activated oxygen hopping was clearly observed from motional narrowing of ^{17}O NMR spectra. The complementary

* Corresponding author at: Institute of Metal Physics, Ural Branch of Russian Academy of Sciences, 620041 Ekaterinburg, Russia. Fax: +7 343 3745244.
E-mail address: verkhovskii@imp.uran.ru (S. Verkhovskii).

0022-4596/$ - see front matter © 2010 Elsevier Inc. All rights reserved.
doi:10.1016/j.jssc.2010.10.029

measurements of the ^{17}O nuclear spin-lattice relaxation rate were performed to clarify peculiar thermally activated hopping of oxygen in the depleted anion sublattice of the LSGM compounds.

2. Experimental

The ceramic specimens $La_{1-x}Sr_xGa_{1-x}Mg_xO_{3-x}$ (LSGM), where $x=0.00$; 0.05; 0.10; 0.12, 0.15; 0.17 and 0.20, were prepared by glycine nitrate synthesis [16]. The typical procedure was as follows. The high-purity lanthanum, gallium and magnesium oxides and strontium carbonate were placed in a quartz glass, and nitric acid was added till complete dissolution was achieved at moderate heating of the starting reagents. Then, glycine (amino acetic acid) was added to form viscous gel. The gradual heating resulted in thickening, solidification and ignition of the desiccated material. The combustion product was ground and subjected to 10 h calcination at 900 °C. The obtained white powder was pressed into pellets and fired at 1400 °C during 10 h. The baked pellets were again crushed into powder with an average grain size of ~20 μm. In order to obtain ^{17}O isotope enriched samples the powder material was treated at 800 °C during 10 h in a flow of gas mixture containing 15vol% of ^{17}O isotope. Then, the specimen was cooled down to room temperature with the rate of 15 °C per hour.

The X-ray powder diffraction patterns (Shimadzu 7000S, Cu$K\alpha$ radiation) were collected at room temperature to confirm single phase state of the synthesized materials at all x's used. The Rietveld refinement procedure (the FULLPROF package) was used to obtain crystalline lattice parameters.

The two-probe a.c. conductivity measurements were carried out with the help of frequency response analyzer Solartron 1260 by the using of ceramic pellets with a diameter of 5 mm and thickness of 5–7 mm. The platinum metal electrodes were deposited upon opposing flat sides of the pellets.

The ^{17}O and ^{71}Ga NMR measurements were performed in the temperature range 100–670 K with an AVANCE III-500 BRUKER spectrometer operating at 11.7 T. Home-built spectrometers were used additionally in the temperature range 80–400 K at 2 and 9.4 T. A high temperature BRUKER probe was utilized for temperature control above 300 K. The spectra were obtained with a conventional spin-echo technique. Since the ^{17}O and ^{71}Ga NMR powder spectra extend on approximately 1 MHz and up to 8 MHz, respectively, a method of frequency sweeping was used. Each powder spectrum was obtained by summing the Fourier-transformed half-echo signals acquired at equidistant operating frequencies, ν_i, with $\Delta\nu=\nu_{i+1}-\nu_i=100$ kHz. The pulse sequence $(\tau)_X$–t_{del}–$(\tau)_Y$–t_{del}–(echo) was used with a τ-pulse duration of ~1 μs and a radio-frequency amplitude H_{rf}~90 Oe. For ^{71}Ga, it corresponds to $\nu_{rf}\sim110$ kHz and $2\pi\nu_{rf}\tau\sim\pi/4$.

The ^{17}O spin-lattice relaxation rate, T_1^{-1}, was obtained from the central peak of ^{17}O NMR spectrum by the using of the inversion recovery pulse sequence (π)–t–$(\pi/2)$–t_{del}–$(\pi/2)$–t_{del}–(echo) with a fixed $t_{del}\sim70$ μs and a π-pulse of ~2 μs. The nuclear magnetization $M(t)$ was measured as the quantity proportional to the integral of the central peak. The characteristic time of the echo-decay, T_2, was defined as the time corresponding to the $1/e$ decrease of the echo-signal $A(2t)$ compared to starting value.

3. Results and discussion

3.1. Structural characterization and conductivity

The parent compound $LaGaO_3$ was indexed with the orthorhombic *Pbnm* space group. Oxides with $x=0.05$, 0.10 and 0.12 were also orthorhombic with the space group *Ibmm*. Increase of doping to $x=0.15$ resulted in rhombohedral structure (e.g. $R\bar{3}c$) while compounds with $x=0.17$ and 0.20 acquired cubic structure (e.g. $Pm\bar{3}m$). The obtained unit cell parameters versus doping are shown in Fig. 1a together with the reduced perovskite cell parameter, ∂p.

The gallates in Fig. 1 differ by the tilts of structural polyhedra that gradually change and decrease in response to the introduction dopants, appearance of oxygen vacancies and respective randomization of the crystalline lattice. The energy of chemical bonding of oxygen with magnesium cations is larger than for gallium ones as is evidenced by the formation enthalpies for MgO and Ga_2O_3. This observation suggests that oxygen vacancies are expected to mostly reside near gallium thus forming oxygen deficient octahedra $Ga(O_{5/6}\square_{1/6})_{6/2}$. Then, the crystal-chemical formula of the solid solution, which reflects this preference, can be presented as $La_{1-x}Sr_x(GaO_{6/2})_{1-3x}(GaO_{5/2})_{2x}(MgO_{6/2})_x$. Hence, the maintenance of rhombic distortions till $x\approx0.13$ presumes that the orthorhombic structure remains stable till a gallium octahedron $GaO_{6/2}$ is corner shared with four gallium–oxygen octahedra on average. Further structural transformation at $x\approx0.16$ signals that rhombohedral distortions, which are characterized by the Ga-O–Ga bridge angle of ~160°, cannot be tolerated by the structure when the average surrounding of a gallium–oxygen octahedron involves nearly three $GaO_{6/2}$ octahedra. Heavier doping results in so strong disordering of gallium–oxygen octahedra and pyramids that the gallium–gallium bridge angle approaches 180° and the doped derivative acquires the cubic symmetry.

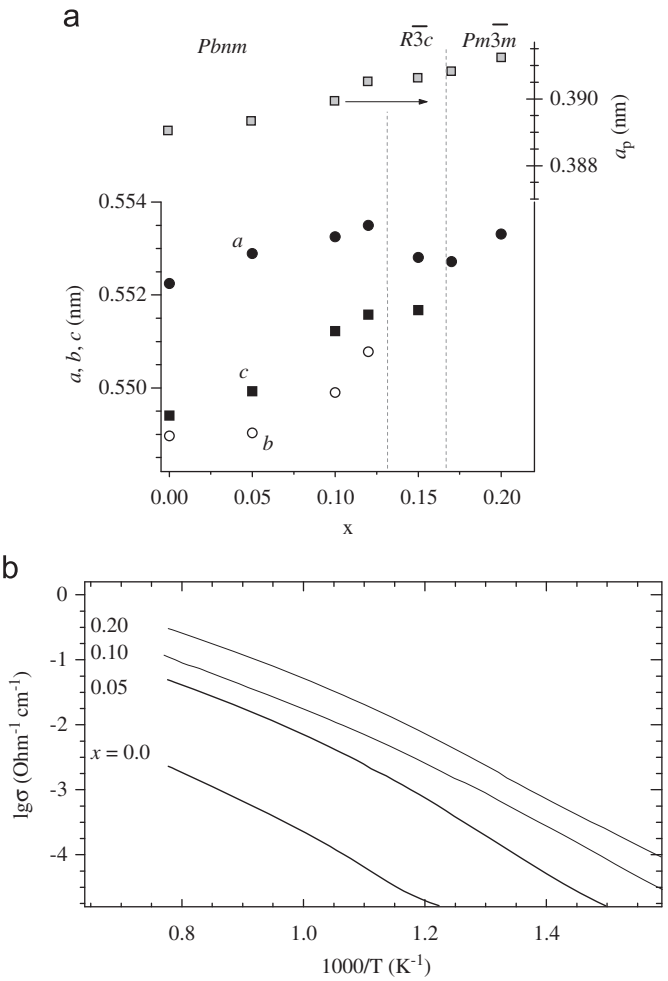

Fig. 1. (a) Room temperature structural parameters a (●), b (○), c (■), a_p in the orthorhombic (*Pbnm/Ibmm*): $a=a_{ortho}$; $b=b_{ortho}$, $c=c_{ortho}/(2)^{0.5}$, rhombohedral (*R3c*): $a=a_{rh}$, $c=c_{rh}/(6)^{0.5}$, and cubic (*Pm3m*): $a=a_c(2)^{0.5}$ phases versus x in $La_{1-x}Sr_xGa_{1-x}Mg_xO_{3-x}$. (b) Arrhenius plots for a.c. conductivity.

The generation of oxygen vacancies in response to doping promotes considerable oxygen ion conductivity in LSGM oxides as can be seen in Fig. 1b where experimental data are shown in Arrhenius coordinates. It is important to notice that the slope of the plots corresponds to apparent activation energy, $E_{a,cond}$, of about 1.0 eV up to ~700 K while it decreases with the temperature increase so that the activation energy equals about 0.7 eV at 1173–1273 K. This behavior is uniform and independent on magnesium doping within the studied range of x's. In order to explain these peculiarities, one can suggest that considerable amount of oxygen vacancies, either in the parent gallate or in the doped derivatives, are trapped in local defect clusters and do not participate in the ion transport at elevated temperature up to ~700 K. The simplest clusters with trapped vacancies can be envisioned as the defect associates, $GaO_{5/2}$-□-$GaO_{5/2}$, while oxygen ion transport is maintained by the residual random vacancies or, in terms of structural polyhedra, by randomized oxygen deficient octahedra $Ga(O_{5/6}□_{1/6})_{6/2}$. The activation energy difference of about 0.3 eV between "low" and "high" temperature limits can be related to a gradual decay with heating of defect associates $GaO_{5/2}$-□-$GaO_{5/2}$ with the release of mobile oxygen vacancies. According to this supposition the doping impacts the population of trapped and mobile vacancies while it does not influence the location near gallium of both vacancy types. This hypothesis is also supported by the shape of the curves in Fig. 1b, which is independent on doping.

The oxygen conductivity level in the parent gallate $LaGaO_{3-\delta}$ achieves about 0.02 Ω^{-1} cm^{-1} at 1273 K, which is 20 times smaller than in $La_{0.95}Sr_{0.05}Ga_{0.95}Mg_{0.05}O_{2.95}$. Therefore, oxygen deficiency in $LaGaO_{3-\delta}$ can be evaluated as $\delta \approx 0.05/20 = 0.0025$. This small non-stoichiometry is most possibly related with partial evaporation of gallium oxide during high-temperature treatments.

3.2. Electric field gradient at Ga-site and vacancy ordering

The presence of oxygen vacancies in LSGM yields the existence of cation sites with lower coordination environments than those of the bulk. These different environments are studied here via the nuclear quadrupolar interaction.

The ^{71}Ga NMR spectrum measured at $H_0 = 9.4$ T and $T = 100$ K is shown in Fig. 2 for some representative compositions, $x = 0$ ($LaGaO_3$), $x = 0.05$ and 0.20 (LSGM) of the ceramics. Its width and particular pattern remain unchanged up to room temperature evidencing that in this temperature range there is no observable ionic motion on the NMR time scale ~(0.1–10) μs that would affect the NMR line shape. The nuclear spin of ^{71}Ga is 3/2 so that a quadrupolar interaction is present if the symmetry of the charge environment of the probed nucleus is lower than cubic. In such a case a central line (corresponding to the nuclear transition $m_I = 1/2 \leftrightarrow -1/2$) with two less intense overlapping satellite lines ($m_I = \pm 3/2 \leftrightarrow \pm 1/2$ transitions) are expected. Indeed the NMR spectra display a narrow central line (~5 kHz) and a broad pedestal of two overlapping satellite lines showing the presence of a quadrupolar broadening due to the interaction of the nuclear quadrupolar momentum $^{71}Q = 0.106 \times 10^{-24}$ cm^2 with the non-zero electric field gradient (EFG) at the Ga site. The components V_{ii} of the EFG tensor are defined in the proper axes, X, Y and Z of the tensor. The quadrupolar interaction is defined by only two parameters namely, the quadrupolar frequency $\nu_Q = (3e^2Q/2I(2I-1)h)V_{ZZ}$ proportional to V_{ZZ} and the asymmetry parameter $\eta = |(V_{XX} - V_{YY})/V_{ZZ}|$. The quadrupolar frequency is directly related to the frequency position and the spread of the satellite lines while η specifies the deviation from axial symmetry at the site. In order to determine ν_Q and η the measured NMR spectral intensity was simulated with a calculated one. In this calculation we took into account both the first order (~ν_Q) and the second order (~ν_Q^2/ν_0) quadrupolar interaction corrections to the Zeeman splitting $\nu_0 = \gamma H_0$. In addition, the shape of the satellite lines required to convolute ν_Q, and η with some distribution function. We chose a Gaussian function $G(\nu_{Q,i}; \Delta\nu_{Q,i}; \eta_i; \Delta\eta_i)$. This experimental spread of the spectra ($\Delta\nu_{Q,i}$; $\Delta\eta_i$) is mainly due to the charge disorder at the cation and anion sites in the samples.

Let us analyze each calculated line-i shown by a grey curve in Fig. 2. In $LaGaO_3$ the spectrum (Fig. 2a) is well described with a

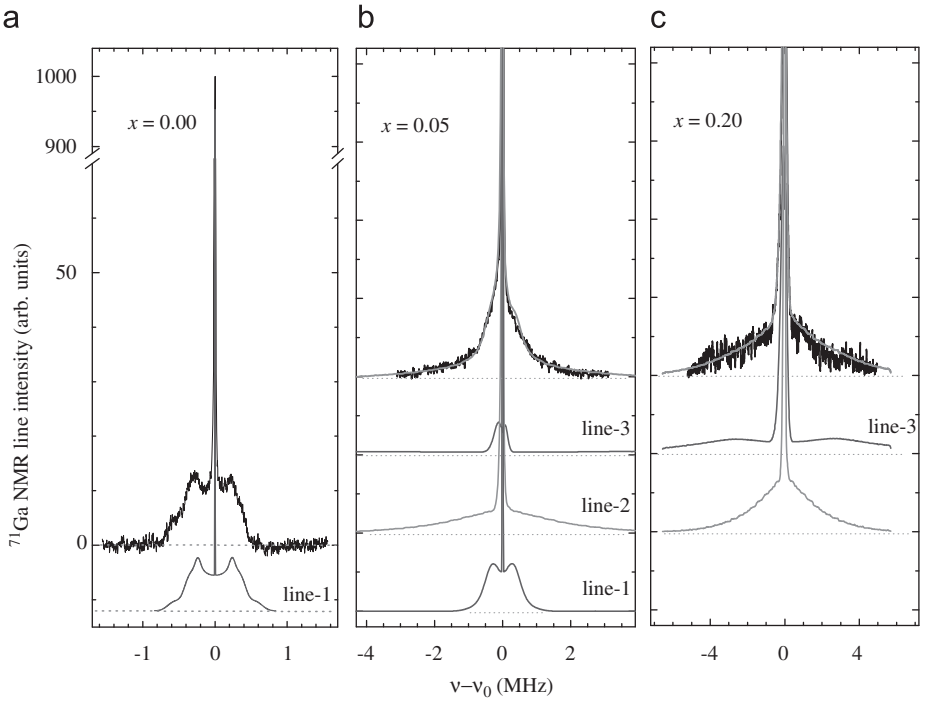

Fig. 2. ^{71}Ga NMR spectra obtained at 9.4 T ($\nu_0 = 54.263$ MHz) and $T = 100$ K in $La_{1-x}Sr_xGa_{1-x}Mg_xO_{3-x}$ ceramics. Line-1–line-3 are the peaks which compose the experimental quadrupole broadened spectra (see text). For $x = 0.05$ and 0.2 the simulated spectrum is shown by a grey-colored line superimposed to the experimental one.

single line, line-1, which parameters are $\{\nu_{Q,}; \Delta\nu_Q\}=(0.67; 0.04)$ MHz and $(\eta; \Delta\eta)=(0.28; 0.06)$. These parameters are assigned to the six-fold coordinated gallium sites (Ga_{VI}) since nominally there is no oxygen vacancy in this compound. The very small broadening $\Delta\nu_Q\sim0.06$, ν_Q deduced from the spectrum simulation indicates a high degree of atomic order in the cation and anion sublattices. The EFG parameters are consistent with those obtained by modeling the second order quadrupolar splitting of the central transition in $LaGaO_3$ [9,11].

In LSGM samples the width of the Ga spectra increases as x increases from 0.05 to 0.20 samples although the crystal symmetry becomes cubic *in average* for $x=0.20$. Only the spectrum of the LSGM boundary compositions $x=0.05$ and 0.20 are represented in Fig. 2. A striking feature is that the spectra cannot be described with a single line. At least three lines with different quadrupole parameters are needed to model successfully the experimental spectra of the $x=0.05$, 0.10, 0.15 samples whereas for $x=0.20$, only two lines are required.

Among the lines composing the experimental spectra the one with the largest quadrupolar frequency is the easiest, although time consuming, to determine experimentally since at frequencies very distant from the Larmor frequency, only this line exists with no overlap. The extension of this line at high and low frequency was carefully measured when sweeping the frequency until the echo signal was zero. We find $^{71}\nu_Q\sim8.5$ MHz for this line labeled line-3. This value is about ~13 times larger than $^{71}\nu_Q(Ga_{VI})$ found for GaO_6 octahedra in $LaGaO_3$ (line-1). In order to analyze further the decomposition of the experimental spectra, we performed an EFG calculation at the Ga site of $LaGaO_3$ in the frame of the point charge model using a home-made program code [17]. For that, the following ion charges: La^{3+}, Ga^{3+}, O^{2-} were assumed, the coordinates of the system were taken from X-ray diffraction data [6] and this work, in accordance with the orthorhombic (*Pbnm*) unit cell parameters. The calculation involves the subsequent distanced atomic shells until the EFG contribution of the next involved shell $|(V_{zz})_n|$ becomes three orders of magnitude smaller than the total EFG value.

Then, several cases of Ga sites with and without oxygen vacancy in their two first anion shells were considered. The first case concerns a single oxygen vacancy (V_O) as a nearest neighbor of Ga (Ga_V) in the orthorhombic LSGM. We find $^{71}\nu_Q(Ga_V)\sim12\,^{71}\nu_Q(Ga_{VI})$, the result is almost the same for a vacancy in the apical O1 and in the equatorial O2 sites and is very close to the experimental finding for line-3. We then considered the case of two adjacent oxygen vacancies on the equatorial O2 sites. This case corresponds to a tetrahedrally coordinated Ga_{IV} where the Ga site forms a so-called Brownmillerite-like fragment [7,8]. We find $^{71}\nu_Q(Ga_{IV})\sim0.7\,^{71}\nu_Q(Ga_V)$. Finally, the case of vacancies in the next nearest anion shell was considered. As such a vacancy is farther from the Ga site than in the previous cases the induced EFG is smaller. In this case $\nu_Q=(1.5–3.5)$ MHz depending on the amount of vacancies and their position in the next nearest shell.

Line-3 was thus assigned to the five-fold coordinated Ga_V sites with a single oxygen vacancy in its first oxygen shell. Its spectral weight shows a gradual growth with x. The parameters of line-2 deduced from the simulation are $\nu_Q=3.9$ MHz; $\Delta\nu_Q=3$ MHz. Taking into account the point charge model calculation we suggest that line-2 is due to Ga_{VI} sites having oxygen vacancies beyond the nearest anion shell. As shown in Fig. 2 for each LSGM sample the ^{71}Ga spectrum was successfully modeled with the same three peaks, line-1–line-3 attributed to the Ga sites with distinct oxygen environment within their two first anion shells. According to this EFG analysis the local symmetry of the Ga sites deviates from cubic even in the most doped LSGM compound $x=0.2$ which crystal structure is indexed by X-ray within the *Pm3m* space group.

This complicated EFG distribution found for ^{71}Ga is summarized in Fig. 3 which displays the spectral intensity as a function of $\nu_{Q,}$ taking into account the $\{\nu_{Q,}; \Delta\nu_Q\}$ value of the corresponding line-1 (Ga_{VI})), line-2 (Ga_{VI} sites having some oxygen vacancies beyond the first anion shell) and line-3 (Ga_V sites with a single oxygen vacancy in its first oxygen shell) shown by dotted lines for $x=0.05$. It is worth to underline that a reasonable simulation of the quadrupole broadened spectrum for all x is achieved with these three lines keeping constant the corresponding quadrupole parameters (ν_{Qi}; $\Delta\nu_{Qi}$) and changing only their relative intensity, Int_i. With the condition $\Sigma_i Int_i=1$, the relative intensity of each line yields a good estimate of the fraction of the corresponding oxygen vacancy configurations in the two nearest anion shells around the distinct Ga sites.

Some caution is required to obtain quantitative spectra from quadrupolar nuclei. For ^{71}Ga ($I=3/2$) spectra, apart from the frequency region of the central line, only the satellites lines ($+1/2\leftrightarrow+3/2$ or $-1/2\leftrightarrow-3/2$ transitions) exist so that the excitation $\nu_{rf}(\nu_{rf}\ll\nu_Q)$ is selective. Thus, the nutation angle is not dependent on ν_Q-value [18]. The chosen pulse duration allows a quantitative comparison of the echo intensity of the satellite lines for nuclei with different ν_Q. Among the crystallites contributing to the frequency region around the central line some have such an orientation that their quadrupolar splitting may be less than ν_{rf}. The echo intensity of these crystallites

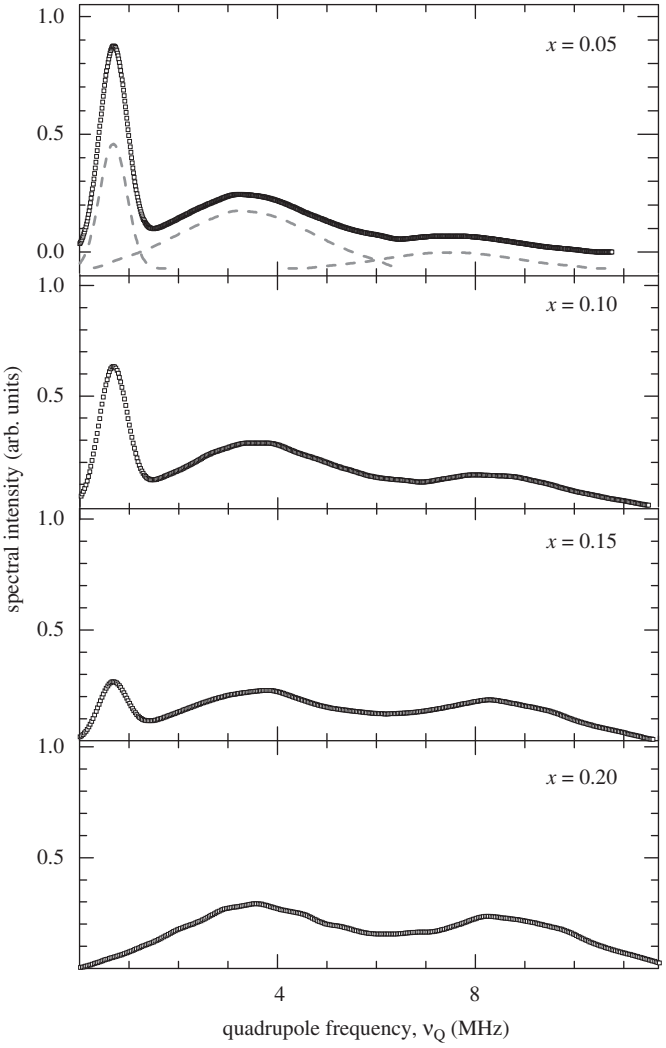

Fig. 3. EFG distribution spectral intensity at gallium sites versus $^{71}\nu_Q$ in $La_{1-x}Sr_xGa_{1-x}Mg_xO_{3-x}$ ceramics. The dashed lines in the uppermost plot belong to the three different Ga environments.

depends on the pulse duration [19]. This fact was taken into account when estimating Int_i.

In Fig. 4 the $Int_i(x)$ data plots are compared with the prediction of models assuming either equiprobable or preferred anion sites for the formation of a V_O vacancy near Ga(Mg). The dashed curves represent two binomial probabilities for the Ga_{VI} sites having no vacancy in the two nearest anion shell. The lower curve $(1-x)^{18}$ concerns the case where Ga_{VI}&Mg_{VI} are equiprobable sites whereas for the upper curve $(1-x)^{17}$ the V_O vacancy forms preferentially near the Ga_{VI}. As both predicting curves trace quite well the relative intensity $Int_1(x)$ of line-1, it is not a conclusive parameter to test an eventual ordering of O vacancies.

In contrast, the relative intensity of line-3 $Int_3(x)$ corresponding to the fraction of the Ga_V sites is a sensitive tool to probe an eventual vacancy ordering. The binomial law $6x(1-x)^5$ corresponds to the formation of a V_O vacancy in the first anion shell of the cation assuming that Ga_V and Mg_V are equiprobable sites. It is shown by the dotted curve in Fig. 4. The inconsistency with the experimental data demonstrates that this assumption is not relevant to LSGM compounds. So that we considered the formation of a single V_O vacancy exclusively in the GaO_6 octahedra while the Mg environment is filled. The corresponding probability of such Ga sites, $2x/(1-x)$, is represented by the black solid curve in Fig. 4. As can be seen it fits well the x-dependence of Int_3. We have also considered the existence of tetrahedral Ga_{IV} sites associated to the Brownmillerite structural fragments [8,11]. In particular, for the orthorhombic LSGMs such Ga sites require the formation of two adjacent oxygen vacancies in the equatorial O2 sites. The corresponding probability, $x(1-x)$, is shown by the dotted-dashed curve. The poor quality of the fit (Fig. 4) makes unlikely this type of static V_O order.

The ^{25}Mg NMR spectrum of the most doped $x=0.2$ compound (Fig. 5) provides an additional proof that no vacancies form in the first coordination shell of Mg. In the case of equiprobable Ga_V&Mg_V sites the NMR spectrum of Mg_V site should show a large quadrupole splitting with $^{25}\nu_Q(Mg_V) \approx 2/3\ ^{71}\nu_Q(Ga_V) \sim 5$ MHz since $^{25}I=5/2$; $^{25}Q=0.22\times10^{-24}$ cm^2 thus NMR signal should be detected far away from the central peak. This is not the case since the total spread of the ^{25}Mg NMR spectrum, 0.2 MHz, is far less than for the Ga_{VI} sites in the $LaGaO_3$ parent compound (Fig. 2a). This narrow ^{25}Mg spectrum is inconsistent with the existence of a vacancy in the first anion shell; it is more relevant to Mg_{VI} sites at the center of an oxygen octahedron with cubic symmetry. This small residual

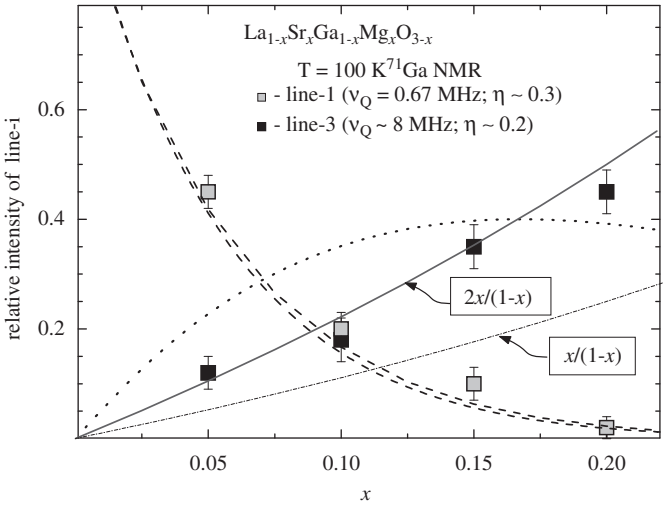

Fig. 4. Comparison of the relative intensity of line-1 and line-3 plotted against x with the prediction of different models for the location of the V_O vacancy nearby Ga(Mg) (see text).

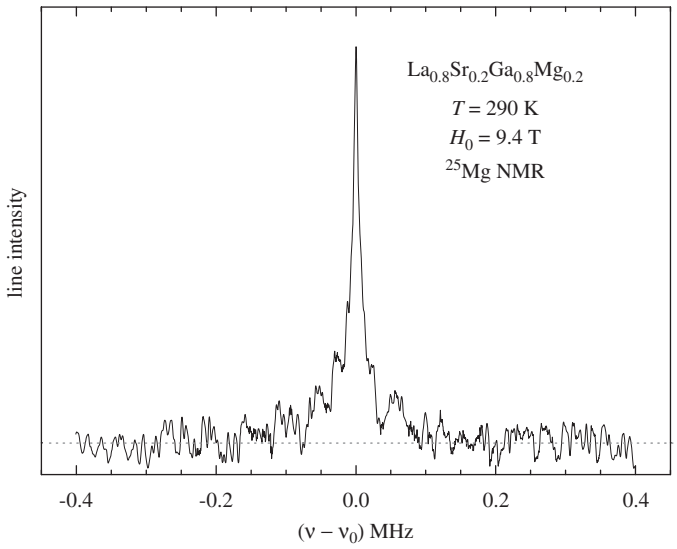

Fig. 5. Room temperature ^{25}Mg NMR spectrum collected at 9.4 T (ν_0=24.48 MHz) in $x=0.2$ LSGM ceramic sample.

quadrupole broadening of 0.2 MHz can be explained naturally by the effect of charge disorder existing intrinsically in the outermost atomic shells of the $x=0.20$ compound. According to the EFG analyses at both, Ga and Mg cations sites we conclude that no vacancies are in the first coordination shell of Mg in LSGM compounds. This conclusion is in agreement with our sample characterization (see Section 3.1) and with recently reported ^{25}Mg MAS NMR data based on chemical shifts. [13].

Above room temperature the quadrupole split structure of the ^{71}Ga spectrum gradually transforms into a single line at $T=500$ K with $^{71}\nu_Q \approx 0$ as shown in Fig. 6. The EFG is the sum of a positive contribution due to the cation charge environment ($^{71}\nu_{Q,cation} \leq 0.5$ MHz) and a negative contribution due to the anion one, $^{71}\nu_{Q,anion} = -|^{71}\nu_{Q,anion}|$. With increasing temperature $|^{71}\nu_{Q,anion}|$ decreases as the oxygen mobility increases whereas $^{71}\nu_{Q,cation}$, the contribution of the immobile cations, is almost constant. The EFG vanishes if $^{71}\nu_{Q,cation} = |^{71}\nu_{Q,anion}|$. In LSGM compounds with two non-equivalent O1 and O2 sites the cancellation the ^{71}Ga EFG depends on the motion of the oxygen vacancies. A hopping restricted to the structurally equivalent O2 sites, i.e. an anisotropic 2D motion should only diminish the anisotropic EFG part $\sim(V_{XX}-V_{YY})$ with no substantial variation of $^{71}\nu_Q \sim V_{ZZ}$ at the Ga sites. Whereas a 3D hopping including the two non-equivalent O1 and O2 sites can completely suppress $^{71}\nu_{Q,anion}$ at high temperature. Thus only the latter motion yields the vanishing of $^{71}\nu_Q = {}^{71}\nu_{Q,cation} - |^{71}\nu_{Q,anion}|$ at some lower temperature. This is the case for the $x=0.05$ compound shown in Fig. 6 where $^{71}\nu_Q$ becomes zero at $T=450$ K whereas the quadrupole splitting reappears at higher temperature. This is also observed for $x=0.10$. In LSGM compounds with equivalent O sites a 3D hopping including all O sites will completely suppress $^{71}\nu_{Q,anion}$ at high temperature.

Thus according to the variation with x of the first order quadrupole split ^{71}Ga spectra in the rigid lattice and to the cancellation of $^{71}\nu_Q$ at elevated temperature the oxygen vacancies are located exclusively nearby Ga. The vacancies are separated from each other. These EFG findings are consistent with a scenario of the vacancy ordering suggested in Section 3.1 that yields defect associates—the $GaO_{5/2}$-□-$GaO_{5/2}$ bi-pyramids with trapped isolated oxygen vacancies. The apical O1 sites are the preferred sites for an isolated trapped vacancy in the orthorhombic LSGM compositions.

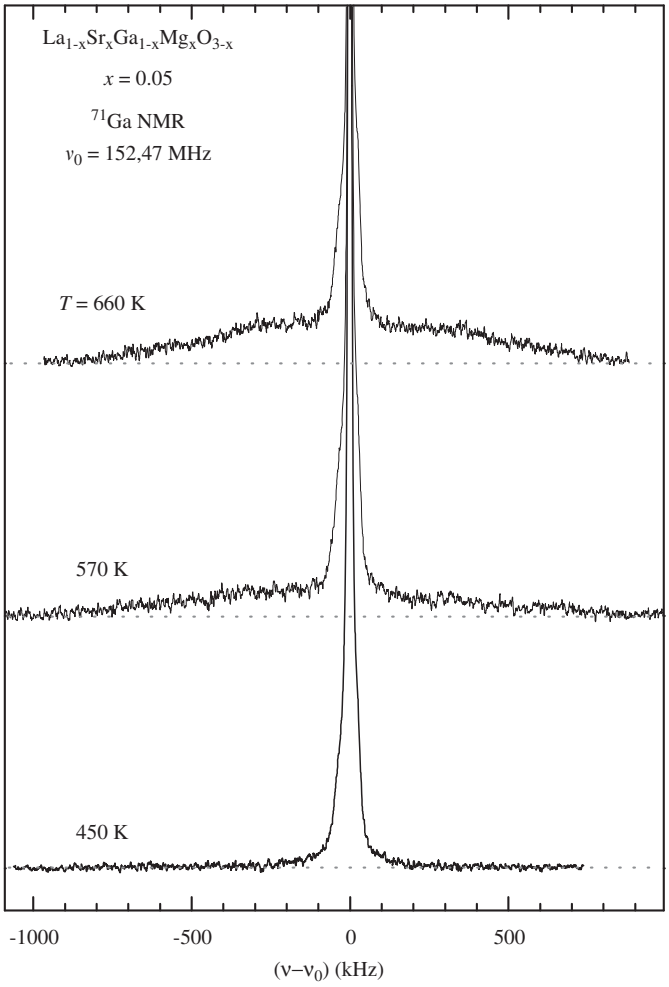

Fig. 6. ^{71}Ga NMR spectra at 11.74 T (ν_0=152.47 MHz) obtained at elevated temperatures in x=0.05 LSGM sample.

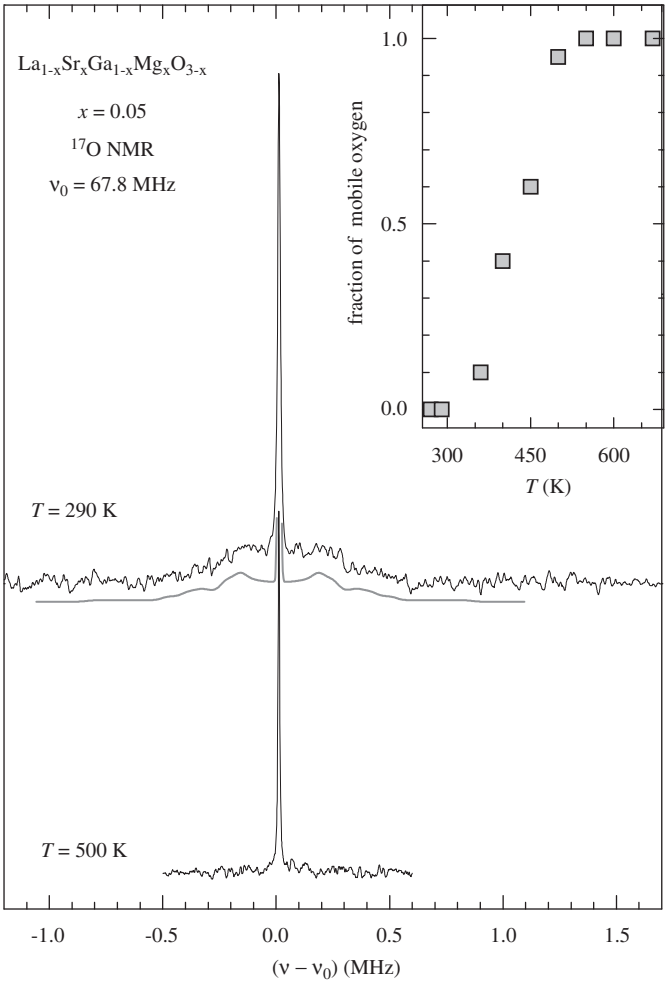

Fig. 7. ^{17}O NMR spectra obtained at 11.74 T (ν_0=67.8 MHz) in LSGM (x=0.05) sample at T=290 and 500 K. The grey line is the corresponding fit. The inset shows the fraction of the mobile oxygen atoms forming the *motional narrowed* line with a vanished static quadrupole splitting.

3.3. Oxygen mobility in ^{17}O NMR spectra and ^{17}O nuclear spin-lattice relaxation

In this section, we focus on ^{17}O NMR to study the effects of the static and dynamics quadrupole interaction created by the thermally activated motion of oxygen. In the orthorhombic structure of LSGM compounds ($x<0.15$) the oxygen atoms occupy two sites. At both sites the symmetry of the charge environment sites is non-axial. The EFG principal ***OZ*** axis at the apical O1 site is parallel to ***a*** or ***c*** orthorhombic axes whereas at the equatorial O2 sites ***OZ*** is nearly directed along $\boldsymbol{r}_{\mathrm{Ga-Ga(Mg)}}$. The slight differences in the Ga–O–Ga bond angles and in the Ga(Mg)–O distances [3,4,8] do not allow to resolve the NMR line corresponding to these sites in polycrystalline samples.

In contrast to ^{71}Ga NMR the quadrupole spread of the ^{17}O NMR spectra is almost unchanged with x, even for the x=0.2 compound which has in average the cubic structure. A representative room temperature ^{17}O NMR spectrum (^{17}I=5/2) acquired at H_0=11.7 T in the x=0.05 sample is shown in Fig. 7. The spectrum displays a narrow central line ($\sim$10 kHz) shifted to $^{17}\delta$=190(20) ppm superimposed on a broad pedestal formed by the four satellite lines. The simulation (grey curve on Fig. 7) of the quadrupole broadened spectrum is obtained with a single set of quadrupole parameters $^{17}\nu_{\mathrm{Q}}(\Delta\nu_{\mathrm{Q}})$=0.43(0.04) MHz and $^{17}\eta(\Delta\eta)$=0.23(0.06). For the x=0.2 sample the widths ($\Delta\nu_{\mathrm{Q}}$) and ($\Delta\eta$) of the Gaussian distribution function required to get a proper simulation is only twice larger.

Considering a quadrupole split spectrum of ^{17}I=5/2 spin the theoretical value of the relative intensity of the central peak is $Int_{\mathrm{centr,rigid}}$=9/35 in the rigid lattice for which no atomic motion exists. The simulation of the room temperature ^{17}O NMR spectra yields Int_{centr}=9/35($\pm$1/35)=$Int_{\mathrm{centr,rigid}}$ for all LSGM compounds studied in this work. Above 300 K the relative intensity Int_{centr} starts to increase.

This intensity excess indicates that a fraction of oxygen atoms becomes mobile. These mobile oxygen atoms form the *motional narrowed* line of relative intensity, Int_{motion}, and with a vanished static quadrupole splitting, $^{17}\nu_{\mathrm{Q,motion}}$=0. Indeed, the static EFG part is reduced for the oxygen atoms participating to the hopping between O-sites that have different direction of the EFG principal axis ***OZ*** with respect to $\boldsymbol{H}_0$. The completely vanished static EFG ($^{17}\nu_{\mathrm{Q,motion}}$=0) implies for oxygen atom a case of the random walk throughout all anion sites allowed by the LSGM structure with a time scale of site exchange [20]: $t_{\mathrm{hop}}<(2\pi\,{}^{17}\nu_{\mathrm{Q,rigid}})^{-1}$ i.e. less than 10^{-6} s.

At each temperature the fraction of the mobile oxygen atoms was estimated as the ratio of the motional-narrowed-line intensity to the total intensity of the ^{17}O NMR spectrum. The inset of Fig. 7 shows that above 500 K all oxygen atoms are involved in this motion in LSGM (x=0.05). A very similar *motional narrowing* effect is detected in the ^{17}O NMR spectrum of the other studied samples.

The ^{17}O spin-lattice relaxation rate, T_1^{-1}, bring more details on the motion features. Above 500 K, as the spectra are motional narrowed, all the nuclear transitions are excited by the pulse sequence. The observed recovery of $M(t)$ is almost exponential. In contrast, below 500 K the $M(t)$ recovery shows a multi-exponential behavior due to the partly selective excitation of the quadrupolar split ^{17}O NMR spectrum. In the whole temperature range (295–670 K) only the $M(t)$ data corresponding to long delays, $t > 0.5T_1$, are analyzed and the same fit expression $M(t)=M_{eq}(1-\alpha \exp(-t/T_1))$ is used, in which M_{eq}, α, and T_1 are adjustable parameters. At these long delays $M(t)$ is a single exponential. The deduced α values are listed in Fig. 8 for $T=600$ and 400 K. The T_1^{-1} data collected at 11.7 T ($\nu_0=67.8$ MHz) and 2 T ($\nu_0=11.6$ MHz) are summarized in Fig. 9. The data exhibit pronounced temperature dependence whereas the absolute value of T^{-1} is almost independent on x and the resonance frequency, ν_0. With increasing temperature T_1^{-1} increases following an exponential law $T_1^{-1} \sim \exp(E_{a,nmr}/T)$ with the same value of activation energy $E_{a,nmr}=0.41(2)$ eV of for all compounds. At high temperature the value of $T_1^{-1}(670\ K)=(0.5–0.6)\ m\ s^{-1}$ approaches the one of the spin–spin relaxation rate $T_2^{-1}(670\ K)=0.8(1)\ m\ s^{-1}$. This evidences the regime of *extreme motional narrowing* characterized by a hopping rate t_{hop}^{-1} exceeding ν_0, the Larmor frequency: $t_{hop}^{-1} > 2\pi\nu_0$ [20].

The T_1^{-1} of oxygen atoms involved in hops between anion sites with different EFG direction is mediated by the time-dependent fluctuations of the EFG. In an isotropic case [20]

$$T_1^{-1} = \frac{2\pi^2}{15}(2I-1)(2I+3)(^{17}\nu_Q)^2\left(1+\frac{\eta^2}{3}\right)J(\omega_0) \quad (1)$$

where $J(\omega)$ is the spectral density of the fluctuating EFG where the amplitude of the latter equals the static $^{17}\nu_Q$ value and $\omega_0=2\pi\nu_0$. The case of an unrestricted random-walk of oxygen atoms on equiprobable sites can be described by the classic Bloembergen, Purcell and Pound (BPP) form of the spectral density [21]:

$$J_{BPP}(\omega) = \frac{2t_c}{1+\omega^2 t_c^2} \quad (2)$$

It predicts a maximum of T_1^{-1} at $(2\pi\ ^{17}\nu_0 t_c)\sim 1$ as well as a $T_1^{-1} \sim {}^{17}\nu_0^{-2}$ dependence at temperatures lower than that of the T_1^{-1} maximum. As seen in Fig. 8b none of these predictions is observed. Moreover, the usual Arrhenius law of $t_c=t_0\exp(E_{a,nmr}/k_BT)$ with $t_0^{-1} \sim 10^{13}\ s^{-1}$ taken from the frequency range of the Ga–O stretching and the O–Ga–O bending vibration modes in LSGM

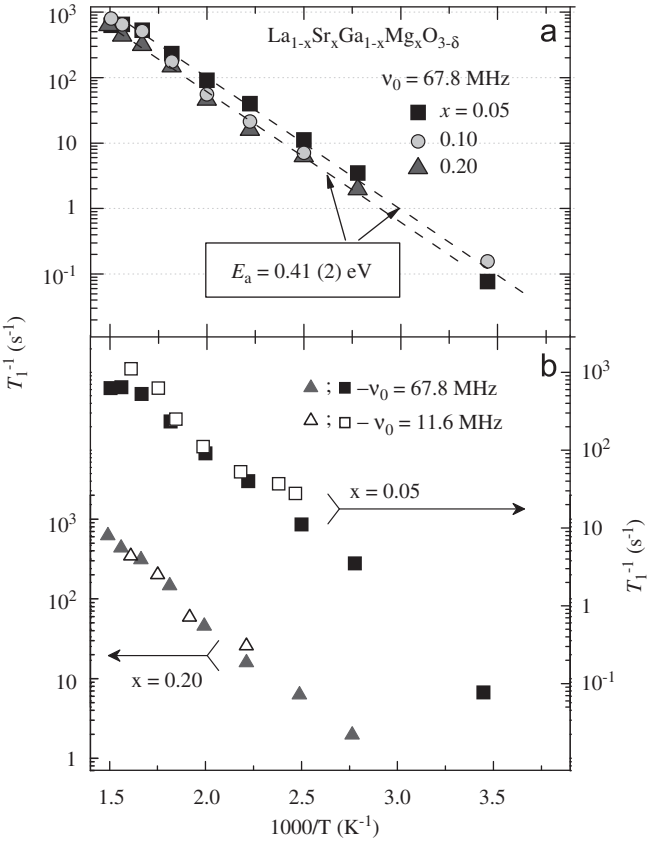

Fig. 9. Arrhenius plots of the nuclear spin-lattice relaxation rate T_1^{-1} measured at different magnetic fields for $La_{1-x}Sr_xGa_{1-x}Mg_xO_{3-x}$, where $x=0.05$; 0.10 and 0.20.

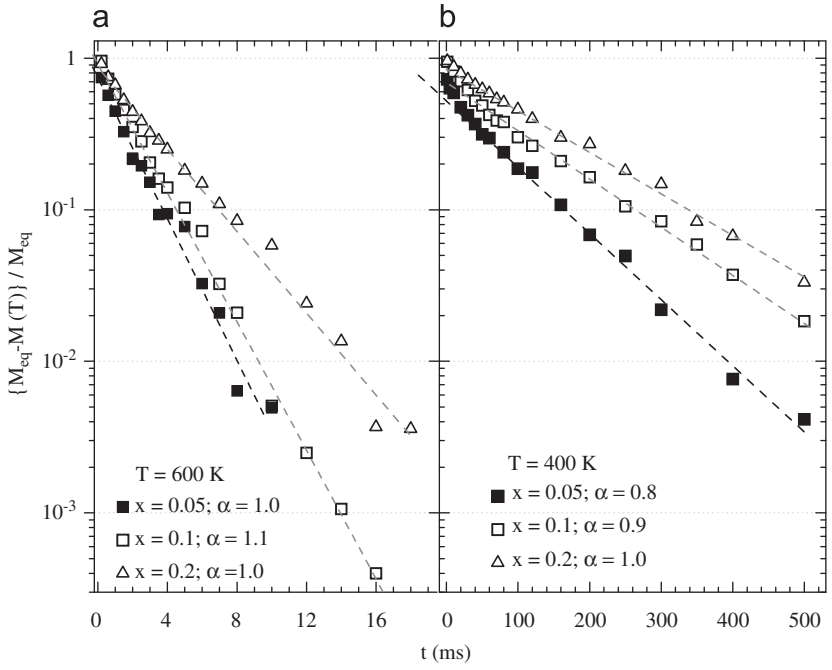

Fig. 8. ^{17}O nuclear magnetization recovery behavior. The data presented in semi-logarithmic scale as $(M_{eq}-M(t))/(M_{eq})$ were obtained at $T=600$ K (a) and 400 K(b). The dashed lines are the corresponding linear fits. The parameter α is explained in the text.

[16] yields with Eq. (1,2) a too fast spin-lattice relaxation rate $T_1^{-1} > 10^3(T_1^{-1})_{exper}$ inconsistent with our data.

A partial loss of randomness of the oxygen hops in the anion sublattice rules out the BPP formalism. Indeed, it is suggested in Section 3.1 and evidenced by ^{71}Ga NMR in Section 3.2 that in the LSGM compounds the vacant anion sites are created mostly inside structural defect associates $GaO_{5/2}$-□-$GaO_{5/2}$ which bi-pyramidal coordination produces vacancies being isolated from each other. The oxygen's walk throughout the anion sublattice should mandatory include hops at the vacant sites, those are the "unpreferred" sites for location of the oxygen. In further consideration of the T_1 behavior we use the formalism of Ref. 22 and label the anion sites preferentially occupied by oxygen as the "*p* sites" whereas the vacant sites, which are unpreferred sites for occupation by oxygen, are labeled as the "*u* sites". The *p* sites have a well depth Δ_p larger than Δ_u of the *u* sites. The nonequivalence of the anion sites results in different probabilities per unit time for a hop from *p* to *u* site W_{pu} (forth) and from *u* to *p* site W_{up} (backwards). At the equilibrium of the thermally activated hopping one get the ratio $W_{up}/W_{pu} \equiv a = \exp(\Delta_p - \Delta_u)/k_BT$.

The high concentration of the preferred sites and the limited amount of the vacant ones allow for rapid local back-and-forth attempts ($\sim W_{up}$) of the oxygen hopping between neighboring *p*–*u* sites but exclude changing the given preferred site. Furthermore, following the pioneer considerations of such correlated hopping problem [22–24] one can get the following expressions for $J(\omega)$ and $E_{a,nmr}$ under the condition $W_{pu} \gg 2\pi\ ^{17}\nu_0$ fulfilled in our ^{17}NMR study:

$$J(\omega) = \frac{2t_c}{1+\omega^2 t_c^2}\,\frac{4a}{(1+a)^2} \tag{3a}$$

$$E_{a,nmr} = 2\Delta_u - \Delta_p \tag{3b}$$

In this scenario of correlated oxygen motion the phonon assisted fast local hopping is the main EFG perturbation mediating the ^{17}I nuclear spin-lattice relaxation, whereas a much longer time $t_{hop} \geq (2W_{pu})^{-1}$ is required for long-distance migrations of the oxygen atom. By applying Eq. (3) to the T_1^{-1} data we obtain an estimate $2W_{pu} \approx 10^{-3}W_{up}$ that means for oxygen about one thousand attempting local hops between successful changes of the preferred site.

Finally, according to Eq. (3) the activation energy estimated from ^{17}O NMR, $E_{a,nmr}$=0.41 eV, is the difference means difference between the well depths of the occupied and the vacant sites. Assuming that the thermally activated long-range migration of oxygen below 700 K is determined with $E_{a,cond} = \Delta_p = 1$ eV we estimate the well depth Δ_u=0.7 eV at vacant sites in LSGM. In the frame of the model Δ_u remains unchanged with doping.

4. Conclusions

The oxygen vacancies distribution and thermally activated motion of oxygen ions have been studied by ^{71}Ga, ^{25}Mg and ^{17}O NMR up to 670 K in $La_{1-x}Sr_xGa_{1-x}Mg_xO_{3-x}$, where x=0.00; 0.05; 0.10; 0.15; 0.20. Additionally, oxygen ion conductivity measurements were carried out up to 1273 K. The comparison of the doped derivatives with the parent gallate $LaGaO_3$ reveals considerable changes in the electric field gradient at Ga sites in the doped samples which are explained by the presence of oxygen vacancies near Ga sites. It is deduced that the temperature decrease results below 500 K in a progressive trapping of mobile oxygen vacancies in bi-pyramids $GaO_{5/2}$-□-$GaO_{5/2}$ and their exclusion from ion transport. The trapped vacancies are separated from each other. This ordering of the trapped vacancies maintains unchanged the nearest octahedral oxygen environment of the magnesium cations at all doping levels.

The onset of thermally activated oxygen hopping is displayed by the motional narrowing of ^{17}O NMR spectra above room temperature. The Arrhenius behavior of the ^{17}O nuclear spin-lattice relaxation rate does not depend on the resonance frequency. This independence indicates two types of oxygen ion motion. Those involve a slow diffusion-type random walk and fast back and forth local jumps of oxygen ions between two adjacent anion sites. These sites are strongly differentiated by the probability of the vacancy formation, like the vacant apical site and the occupied equatorial site in the orthorhombic compositions $x < 0.15$.

A further NMR study of the anion sublattice is required at higher temperature in order to know if the ion conductivity is still entirely related to the presence of oxygen deficient octahedra located randomly in the crystal lattice of $La_{1-x}Sr_xGa_{1-x}Mg_xO_{3-x}$ while the Mg cations maintain their octahedral oxygen environment independently on the doping level.

Acknowledgments

This work is supported in part by the Ural Branch of RAS (Grant 09-M-23-2002 and the Russian Foundation for Basic Research (Grant 10-03-01054). S.V. and A.Y. are grateful to ESPCI and CNRS for hospitality and support.

References

[1] T. Ishihara, H. Matsuda, Y. Takita, J. Am. Chem. Soc. 116 (1994) 3801–3803.
[2] M. Feng, J.B. Goodenough, Eur. J. Solid State Inorg. Chem. 31 (1994) 663–672.
[3] T. Ishihara, H. Matsuda, Y. Takita, Solid State Ionics 79 (1995) 147–151.
[4] J. Drennan, V. Zelisko, D. Hay, F.T. Ciachi, S. Rajendran, S.P.S. Badwal, J. Mater. Chem. 7 (1997) 79–83.
[5] P.R. Slater, J.T.S. Irvine, T. Ishihara, Y. Takita, J. Solid State Chem. 139 (1998) 135–143;
P.R. Slater, J.T.S. Irvine, T. Ishihara, Y. Takita, Solid State Ionics 107 (1998) 319–323.
[6] L. Vasylechko, V. Vashook, D. Savytskii, A. Senyshyn, R. Niewa, M. Knapp, H. Ullmann, M. Berkowski, A. Matkovskii, U. Bismayer, J. Solid State Chem. 172 (2003) 396–411.
[7] A. Skowron, P. Huang, A. Petric, J. Solid State Chem. 143 (1999) 202–209.
[8] M.S. Khan, M.S. Islam, D.R. Bates, J. Phys. Chem. B 102 (1998) 3099–3104.
[9] T.J. Bastow, T. Mathews, J.R. Sellar, Solid State Ionics 175 (2004) 129–133.
[10] D. Massiot, I. Farnan, N. Gauter, D. Trumeau, A. Trokiner, J.P. Coutures, Solid State NMR 4 (1995) 241–248.
[11] J.L. Palumbo, Ph.D. Thesis, Stony Brook University, New York, 2007.
[12] S. Stolen, E. Bakken, C.E. Mohn, Phys. Chem. Chem. Phys. 8 (2006) 429–447.
[13] F. Blanc, D. Middlemass, L. Buannic, L. Holmes, R. Dervisoglu, D.D. Morgan, C.P. Grey, in: Abstracts of the 216th ECS Meeting, 2009, Vienna, Austria, 04-24.
[14] J.F. Stebbins, Science 297 (2002) 1285–1287.
[15] N. Kim, C.P. Grey, Science 297 (2002) 1317–1320.
[16] I.V. Baklanova, I.A. Leonidov, L.A. Perelyaeva, Bull. Russ. Acad. Sci.: Phys. 72 (2008) 1343–1346.
[17] S. Verkhovskii, A. Trokiner, A. Gerashenko, A. Yakubovskii, N. Medvedeva, Z. Litvinova, K. Mikhalev, A. Buzlukov, Phys. Rev. B 81 (2010) 144415.
[18] D. Freude, J. Haase, in: P. Diehl, E. Fluck, H. Guenther, R. Kosfeld, J. Seelig (Eds.), NMR Basic Principles and Progress, vol. 29, Springer-Verlag, Berlin, Heidelberg1993, pp. 3–85.
[19] P.P. Man, J. Chem. Phys. 106 (1997) 3908–3919.
[20] A. Abragam, The Principles of Nuclear Magnetism, Oxford University Press, UK, 1961.
[21] Bloembergen, E.M. Purcell, R.V. Pound, Phys. Rev. 73 (1948) 679–712.
[22] P.A. Fedders, Phys. Rev. B 18 (1978) 1055–1065.
[23] R. Blinc, in: J.S. Waugh (Ed.), Advances in Magnetic Resonance, vol. 3, Academic Press, New York1968, pp. 166–204.
[24] H. Lutgemeier, H.G. Bohn, R.R. Arons, J. Magn. Reson. 8 (1973) 80–86.